



Flow-induced vein-wall vibration in an arteriovenous graft

S.-W. Lee^a, P.F. Fischer^b, F. Loth^{a,c,*}, T.J. Royston^{a,c}, J.K. Grogan^d,
H.S. Bassiouny^d

^aDepartment of Mechanical and Industrial Engineering, The University of Illinois at Chicago, 842 W. Taylor, Chicago, IL 60607, USA

^bMathematics and Computer Science Division, Argonne National Laboratory, 9700 S. Cass Avenue, Argonne, IL 60439, USA

^cDepartment of Bioengineering, The University of Illinois at Chicago, 842 W. Taylor, Chicago, IL 60607, USA

^dDepartment of Surgery, The University of Chicago, 5841 S. Maryland Ave., Chicago, IL 60637, USA

Received 23 September 2004; accepted 27 April 2005

Abstract

The hemodynamic environment of an arteriovenous (AV) graft differs from that of arterial grafts because mean flow rates are typically 10 times greater. This increased flow rate can create a weakly turbulent state, which alters the biomechanical environment greatly and may play a role in AV graft failure. A canine animal study was conducted to simulate the hemodynamic environment of a human AV graft. In vivo measurements were obtained for vein-wall vibration (VWV), graft geometry, and blood flow rate. In order to investigate the complex flow structure at the venous anastomosis of an AV graft, which is thought to induce these vibrations, a computational fluid dynamics study was conducted by direct numerical simulation under pulsatile flow and geometry conditions based on the animal study. The simulation technique employs the spectral element method, which is a high-order discretization ideally suited to the simulation of transitional flows in complex domains. The minimum and maximum Reynolds numbers entering the graft, based on average velocities, were 875 and 1235, respectively. While velocity and pressure fluctuations are clearly present in the numerical simulations, their magnitude and frequency do not correlate well with the in vivo VWV measurements. Potential reasons for this discrepancy are threefold. First, a quiescent inflow condition was used in the present computations; a more realistic inflow condition might alter the velocity fluctuations significantly. Second, simulations were conducted with a rigid geometry; compliance may play an important role in flow stability within an AV graft. Third, the flow split between the graft and vein inlet may also play an important role in the stability of the flow structures.

© 2005 Elsevier Ltd. All rights reserved.

Keywords: Arteriovenous graft; Vein vibration; Direct numerical simulation; Pulsatile flow; Hemodynamics; Blood vessel; Transitional flow

1. Introduction

Individuals with end-stage renal disease would succumb in a few weeks or months if not sustained by dialysis therapy or a kidney transplant. For hemodialysis patients, an arteriovenous (AV) communication (Fig. 1) is constructed from

*Corresponding author. Tel.: +1 312 996 3045; fax: +1 312 413 0447.

E-mail addresses: slee92@uic.edu (S.-W. Lee), fischer@mcs.anl.gov (P.F. Fischer), floth@uic.edu (F. Loth), troyston@uic.edu (T.J. Royston), jgrogan@surgery.bsd.uchicago.edu (J.K. Grogan), hbassiou@surgery.bsd.uchicago.edu (H.S. Bassiouny).

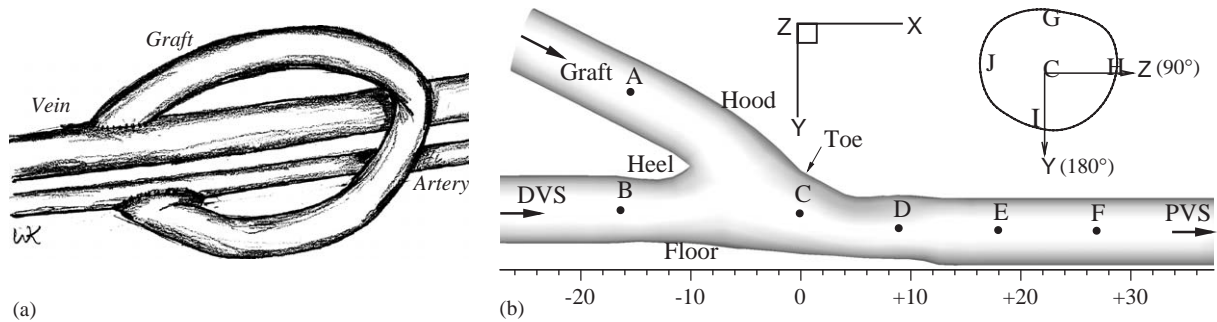


Fig. 1. (a) Sketch of AV graft; (b) nomenclature for AV graft geometry.

an artery to a vein to provide an access site. By bypassing the high-resistance vessels (arterioles and capillaries), high flow rates can be achieved that are necessary for efficient hemodialysis. In the United States, the majority of AV communications are constructed by using polytetrafluoroethylene (PTFE) grafts. Unfortunately, more than half of the AV grafts fail and require surgical reconstruction within three years. The prevalent cause of these graft failures is venous anastomotic intimal hyperplasia (VAIH)—a stenosis, or narrowing of the vein, downstream of the graft (Kanterman et al., 1995). While the natural healing response after surgery causes some degree of intimal thickening, the biomechanical environment appears to be responsible for progression of intimal thickening to occlusive VAIH. Biomechanical forces in the AV graft are similar to those of flow downstream of an arterial stenosis, with generally high wall shear stress (WSS) acting on the vein, flow separation, and pressure fluctuations that vibrate the vein wall and surrounding tissue.

Considerable work has been conducted to elucidate the hemodynamic environment within an AV graft. The time variant velocity profiles and WSS distributions were measured in a transparent elastic AV graft model using laser Doppler anemometry (LDA) and the high flow rate and pressure were shown to generate large vortical structures that significantly altered the normal vein flow conditions (Shu et al., 1987). This study was carried out in an AV loop graft model under pulsatile flow conditions with an average Reynolds number of 1160. Another study by the same group (Shu and Hwang, 1988) described the venous wall vibration, or thrill, generated by pressure fluctuations to be a common characteristic of most of clinical AV grafts and showed a dominant frequency of approximately 100 Hz as measured by phonoangiography. Both in vitro experimental and computational studies by Loth et al. (2003) revealed significant levels of velocity fluctuations for Reynolds number 1820 in an idealized model of an AV graft. However, the researchers found no evidence of velocity fluctuations at Reynolds number 1060. In addition, they reported measurements of significant in vivo vein-wall vibration (VWV) on a porcine model. Using a computational fluid dynamics (CFD) method, Ene-Iordache et al. (2001) examined the fluid dynamics of a patient-specific end-to-end AV fistula with Reynolds numbers ranging from 658 to 1275. The high flow rate and sharp bend of the radial artery upstream of the venous anastomosis caused the vessel wall to be subjected to high WSS, flow recirculation, and areas of elevated WSS gradients. The researchers did not report transitional flow. Another study (Sivanesan et al., 1999) observed high-intensity turbulence near the venous anastomosis in an AV fistula, although the geometry (direct connection of artery and vein, end-to-side) differs from the one in the present study. Ethier et al. (2000) described detailed separation patterns in a 45° junction that resembles the venous anastomosis for Reynolds numbers in the range 250–1650. Transition to unsteadiness was observed experimentally at $Re = 1650$ but not at $Re = 1100$. However, the numerical simulations were confined to the steady laminar flow regime.

Only a few studies can be found in the literature of numerical simulation for transitional flow in a physiological geometry (Mallinger and Drikakis, 2002; Mittal et al., 2003). Mittal et al. (2003) investigated the turbulent flow physics through the simple arterial stenosis using CFD. They carried out direct numerical simulations and large-eddy simulations for pulsatile flow in a channel with a one-sided semicircular constriction over a range of Reynolds numbers from 750 to 2000 with a rigid wall assumption. This study showed large fluctuations in wall pressure and shear stress downstream of the constricted region, and the frequency was found to be associated with the periodic formation of vortex structures in the shear layer for Reynolds number greater than 1000.

While only a few CFD studies have examined turbulent flow in physiological geometries, significant CFD research has focused on vortex-induced vibration in flow over a cylinder, both for two-dimensional (2-D) laminar flow (Guilmineau and Queutey, 2000; Shiels et al., 2001) and three-dimensional (3-D) turbulent flow (Evangelinos and Karniadakis, 1999).

Considerable attention has been given to the effects of biomechanical factors, especially tissue wall vibration, on the development and progression of poststenotic dilatation (PSD). An early study of PSD showed that thrills have a correlation with dilatation development (Roach, 1963). Subsequent studies demonstrated that isolated arteries dilate when subjected to mechanical vibrations at frequencies from below 100 to over 200 Hz (Boughner and Roach, 1971). Foreman and Hutchison (1970) demonstrated that fluid flow through isolated arteries with a forced stenosis excites the artery wall over a wide range of frequencies and that the frequencies of the peak wall-vibration correspond closely to resonant frequencies of the artery wall. Ojha and Langille (1993) reported that PSD can occur under turbulence-free conditions. This arterial response is in contrast to veins exposed to turbulence. In vivo studies in a canine AV graft model have shown that perivascular tissue vibration is correlated with VAIH ($r = 0.92$, $p < 0.001$) (Fillinger et al., 1990); the authors hypothesized that the tissue vibration was caused by turbulent flow, because the Reynolds numbers were near the critical value of 2100. While the biological responses to turbulence and wall vibration in blood vessels have been reported, further research is necessary for a complete understanding of the biomechanical mechanisms involved.

The present study examines detailed flow structures and fluctuations in the venous anastomosis of one AV graft by employing direct numerical simulation. The simulations are conducted on the in vivo graft geometry under in vivo pulsatile flow conditions obtained from an animal study. We present in vivo VWV measurements and CFD simulation results. The velocity and pressure fluctuations from the simulation are compared with the in vivo measurements.

2. Methods

2.1. Experimental method of in vivo study

A mongrel dog weighing about 25 kg was studied for in vivo vibration and volumetric flow rate measurements. During the canine animal surgery, a 6 mm diameter PTFE graft (W.L. Gore & Associates, Inc., Flagstaff, AZ) was implanted from the femoral artery to the femoral vein in a standard end-to-side anastomotic fashion using 6-0 Gore-Tex suture (W.L. Gore & Associates, Inc.). Housing and handling of the animal was in compliance with “Guide for the Care and Use of Animals” (National Academy of Sciences, copyright 1996). Volumetric flow rate was measured in the distal and proximal outflow tracts by a transit time ultrasound flow meter (Transonics Systems Inc, Ithaca, NY). VWV was measured at defined anastomotic regions on the vein (every 5 mm) by a noncontacting laser Doppler vibrometer (LDV, Polytec PI Inc., CLV-800, Waldbronn, Germany). The analog signal from the LDV, which is proportional to vein-wall radial vibration velocity, was digitized at a sampling frequency of 2048 Hz and recorded (without windowing) by using a PC-based data acquisition card (National Instruments Corporation, Austin, TX). The amplitude spectra of VWV were obtained by fast Fourier transform (FFT) of the time signal in Matlab (The Mathworks, Inc., Natick, MA). The amplitude spectrum can be calculated by the FFT multiplied by its complex conjugate and square rooted. In order to quantify the flow-induced vibration level as a single number, the root-mean-squared value of the vibration velocity amplitude in the frequency range 40–800 Hz was calculated based on the digitized time record, which was band-pass filtered by using a Butterworth band-pass filter (order = 12) implemented in Matlab.

After in vivo measurements were complete, the animal was sacrificed with an overdose of sodium pentobarbital. The PTFE graft was cannulated, and the venous outflow tract was perfusion fixed with 3% glutaraldehyde at 100 mmHg for 15 min. This process preserves the tissue but does not maintain the geometry of the anastomosis. The proximal and distal venous segments were then clamped approximately 7 cm from the anastomosis, taking care to keep the anastomosis in its in situ position, without stretching or twisting the anastomotic geometry. The PTFE graft was transected 7 cm from the venous anastomosis. Small incisions (<2 mm) were made in the vein adjacent to the clamps, and blood was evacuated from the transected graft and isolated vein. The clamped vein was then rinsed with saline. Vinyl polysiloxane (3M Company, St Paul, MN) was injected with a 3M ESPE dispenser through the graft, until the vein was expanded fully and excess polysiloxane exited via the small incisions. The filling pressure was not monitored. However, filling to the point of a fully expanded vein closely mimics the in vivo geometry of the anastomosis, since veins are known to have low compliance at arterial pressures [less than 0.1%/mmHg for canine femoral vein at 60 mmHg (Brossollet, 1992)], and PTFE have even smaller compliance [0.01%/mmHg for PTFE at 60–150 mmHg (Brossollet, 1992)]. After the vinyl polysiloxane hardened, the graft and vein were explanted.

2.2. Geometry and computational mesh

The perfusion-fixed plastic cast of the canine venous anastomosis was scanned by using a computerized tomography (CT) scanner (GE Medical Systems, UK). This produced gray-scale images of the graft sliced axially (23 images,

512 × 512, FOV = 97 mm × 97 mm, slice thickness = 1.25 mm). From these slice-based images, the 3-D geometry was reconstructed with commercial image-processing software (Mimics, Materialise, Belgium).

The graft, distal vein segment (DVS) inlet, and proximal vein segment (PVS) outlet diameters were 6, 6, and 6.5 mm, respectively (note these are only approximate because cross-sections were not perfectly circular). The actual geometry obtained from CT had extended only 12.5 mm beyond the toe and 4.5 mm beyond the heel of the anastomosis. In order to create a larger computational domain, two extensions were added to the proximal and distal ends of the vein of 23 and 12.5 mm, respectively. The extension at the proximal end consisted of repeated contours based on the final contour. At the distal side, the final contour was expanded gradually (over ~2 mm) to a 6 mm diameter circular cross-section. The resulting 3-D geometry was smoothed by using previously described FORTRAN software (Yedavalli et al., 2001). The method uses a moving average technique in the circumferential and axial directions with a window size of 10 points (0.4 graft diameters) and 10 points (0.25 graft diameters), respectively. A 3-D computational mesh was created based on this smoothed surface data by using a technique described previously (Lee et al., 2000). In order to generate a high-quality hexahedral mesh, an isotherm surface was used from a heat conduction-based algorithm, which guarantees orthogonality of elements to the wall boundary with minimal deformation for complex bifurcation geometries and smoother transition of element shape at the bifurcation region (Lee, 2002; Lee et al., 2002a), by demonstrating that the site of PSD was remote from that of the localized turbulence zone. The mesh comprised $K = 2640$ hexahedral elements in an O-grid pattern shown in Fig. 2. For the spectral element method of polynomial order of 12, each macro mesh has 2197 ($13 \times 13 \times 13$) locally structured node points. Thus, while the mesh has a small number of elements, the total number of grid points is much larger ($\sim 2640 \times 12 \times 12 \times 12 = 4,561,920$). This spectral element approach also provides exponential rates of convergence for a sufficiently smooth solution.

2.3. Computational method

The spectral element method (SEM), which is a high-order weighted residual technique, was used to solve the 3-D unsteady incompressible Navier–Stokes equations with a rigid wall assumption,

$$\frac{\partial \mathbf{u}}{\partial t} + \mathbf{u} \cdot \nabla \mathbf{u} = -\frac{1}{\rho} \nabla p + \nu \nabla^2 \mathbf{u}, \quad (1)$$

$$\nabla \cdot \mathbf{u} = 0. \quad (2)$$

Here, p is the pressure, and ν is the kinematic viscosity of the fluid. Dirichlet boundary conditions (based on Womersley flow) are specified at the vessel inlets, and Neumann boundary conditions are prescribed at the outlet.

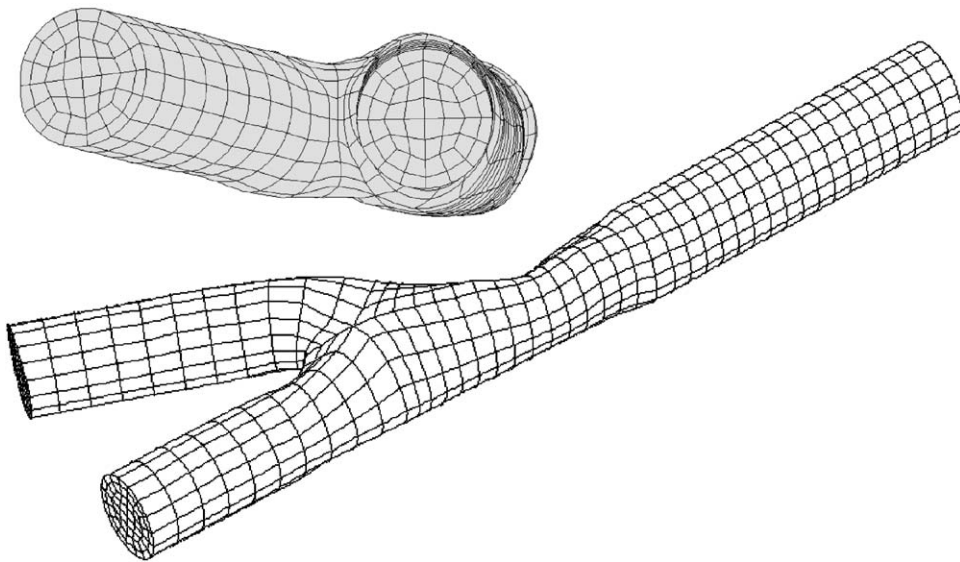


Fig. 2. Spectral element mesh for AV graft ($K = 2640$).

Spatial discretization is based on the $P_N - P_{N-2}$ spectral element method (Maday and Patera, 1989; Fischer, 1997), which uses compatible velocity and pressure spaces that are free of spurious modes. Within each of K elements, velocity and pressure are represented in local Cartesian coordinates by tensor-products Lagrange polynomials of degree N and $N - 2$, respectively. These Lagrange interpolants are based on Gauss–Lobatto–Legendre quadrature points for velocity and Gauss–Legendre quadrature points for pressure. For problems having a smooth solution, the discretization error of the SEM decreases exponentially with N , resulting in minimal numerical dispersion and diffusion.

The temporal discretization of the Navier–Stokes equations is based on second-order operator-splitting methods (Maday et al., 1990). The convective term is expressed as a material derivative, which is discretized by using a stable backward difference scheme

$$\frac{\tilde{u}^{n-2} - 4\tilde{u}^{n-1} + 3\tilde{u}}{2\Delta t} = S(\tilde{u}), \quad (3)$$

where $S(\tilde{u})$ is the linear symmetric Stokes problem to be solved implicitly and \tilde{u}^{n-q} is a velocity field at time step $n-q$, computed as the explicit solution to the pure convection problem. The subintegration of the convection term permits values of Δt corresponding to convective Courant numbers of 1–5, thus significantly reducing the number of (expensive) Stokes solves. Further details on the computational solution technique may be found in Fischer et al. (2002).

3. In vivo measurements

3.1. Flow rate in the vein

The flow waveform for the animal study of interest is shown in Fig. 3 for 12 cardiac cycles. The mean flow rate is +1036 ml/min in the PVS and +39 ml/min in the DVS (range +807 to +1320 and –114 to +93 ml/min, respectively). A characteristic feature of the AV graft flow rate is that its mean flow rate is large relative to its peak-to-peak oscillation during the cardiac cycle.

3.2. Vein-wall vibration

The time traces of VWV shown in Fig. 4 indicate greater vibration downstream of the toe than upstream. In Fig. 5, the corresponding VWV power spectra show that the largest vibration is within the range of 100–250 Hz at the downstream site (10 mm downstream of the toe). The variation along the vein is shown to increase with axial position in the downstream direction (Fig. 6).

4. Numerical simulations

Flow simulations were conducted on the NSF Pittsburgh Supercomputing Center TCS1 with 256 plus 1024 parallel processors (P). The simulations were initiated at $Re \ll 1$, and the Reynolds number was ramped up to the diastolic value by exponentially decreasing the viscosity. After initialization, the flow problem was simulated for six cardiac cycles with a polynomial degree of basis function $N = 12$ (total simulation was 85 h with $P = 256$ plus 50 h with $P = 1024$).

The volumetric flow rates measured in DVS and PVS during the animal study were phase-averaged for 12 heartbeat cycles. Flow rate in the graft was obtained as the difference between the PVS and DVS outlet. The blood flow waveforms that were used as boundary conditions for the graft and DVS inlets during each cardiac cycle are shown in Fig. 3(b). These flow waveforms were imposed as velocity boundary conditions with a Womersley solution, an analytic solution of laminar, fully developed pulsatile flow on both inlet boundaries (Womersley, 1957). The minimum and maximum Reynolds numbers entering the graft, based on averaged velocities (over the cross-section) and graft diameter were 875 and 1235, respectively.

4.1. Flow physics

The instantaneous velocity vectors on the mid-plane in x – y coordinate at systolic (maximum graft flow rate) and diastolic phase (minimum graft flow rate) are shown in Fig. 7. The velocity vectors are qualitatively similar between the systolic and diastolic phase because of the large mean velocity component and low pulsatility of the inlet flow condition. The axial velocity profile is skewed toward the outer wall forming a jet flow in the PVS. The low velocity is observed

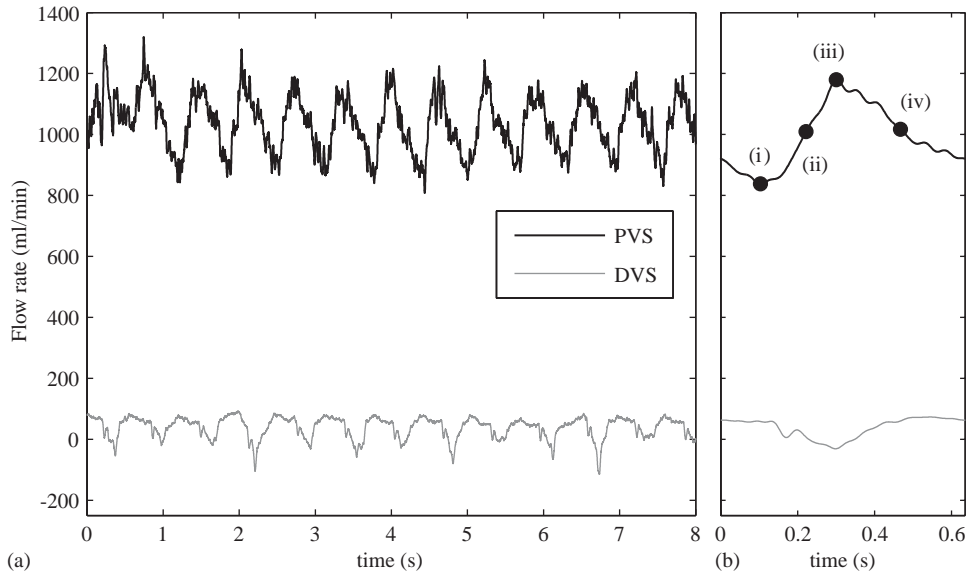


Fig. 3. Flow rates in the PVS and DVS: (a) in vivo measurements; (b) phase-averaged flow wave forms used as the inlet boundary conditions for the numerical simulation.

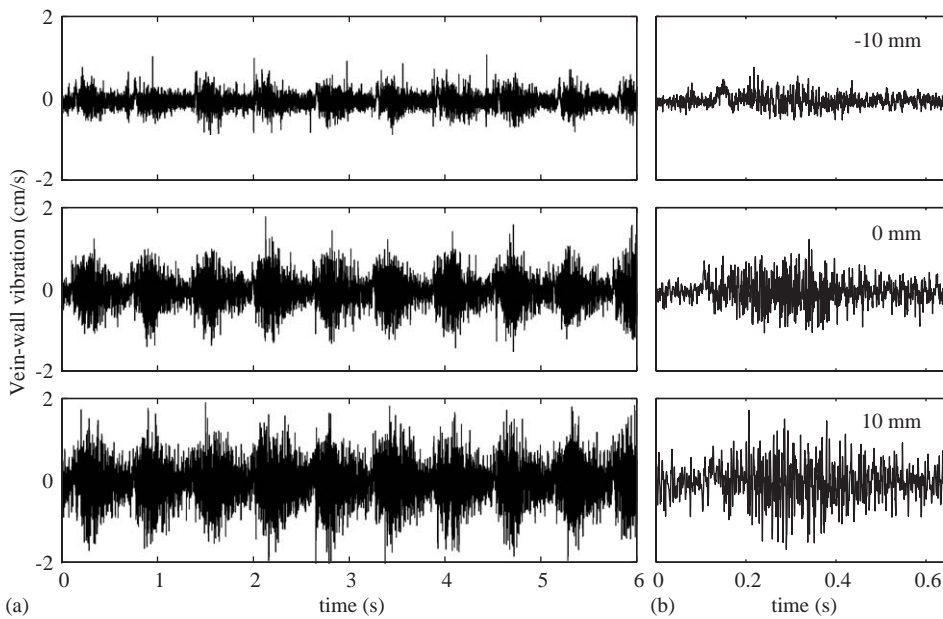


Fig. 4. Time trace of vein-wall vibration (VWV) measured in vivo after graft construction: (a) full record; (b) one cycle. Distance is measured from the toe (positive: PVS; negative: DVS).

near the centerline of the PVS, as is commonly found with strong Dean flow. In addition, the out-of-plane nature of the graft inlet induces a large swirl, which results in an asymmetric Dean flow pattern in the PVS. The distribution of axial velocity magnitude is shown in Fig. 8 as contour plots of the cross-section at four axial locations (C, D, E, and F). These plots are given at four time points during the cardiac cycle, which correspond to minimum flow rate, mid-acceleration,

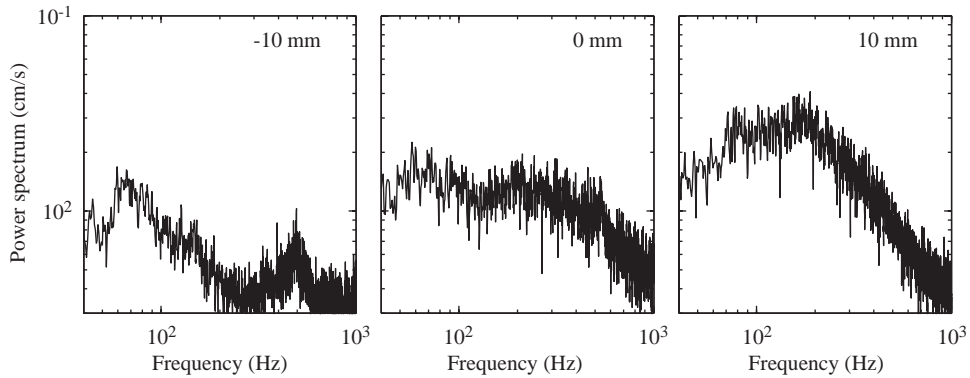


Fig. 5. Frequency spectra of VVW measurement taken in vivo after graft construction.

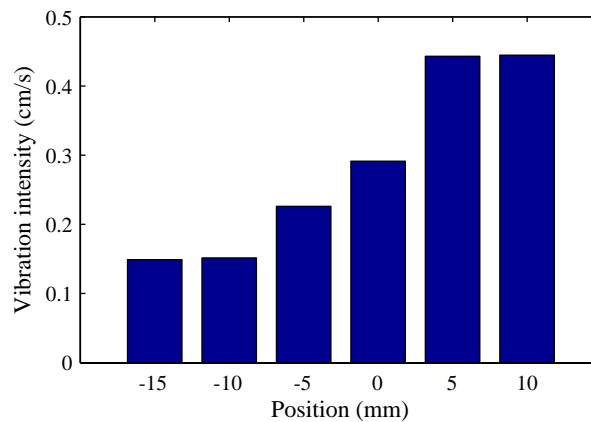


Fig. 6. Vibration intensity for six axial positions along the vein from in vivo measurements.

maximum flow rate, and mid-deceleration. The axial nature of the flow in the PVS is illustrated in Fig. 9 by coherent structures (vortices) identified by using the criterion of Jeong and Hussain (1995).

4.2. Fluctuations in the flow

Fig. 10 shows the fluctuations in velocity magnitude at the axial positions A–F indicated in Fig. 1. The corresponding power spectra are given in Fig. 11. The velocity fluctuations in the graft and DVS (upstream of the anastomosis) are low frequency and are dominated by the pulsatile input associated with the cardiac cycle. A cascade to small flow scales as one proceeds downstream of the anastomosis is indicated by the increased high-frequency content in Figs. 10 and 11 at stations D, E, and F. Figs. 12 and 13 show the corresponding time traces and power spectra for the pressure. We note that Figs. 10 and 12 indicate complete repeatability of the flow from one cardiac cycle to the next, even at the downstream stations E and F.

4.3. Wall pressure distribution

Time-averaged and r.m.s. values of the axial pressure distributions are shown in Fig. 14. The time-averaged pressure distribution along the centerline of the flow axis from the graft to the PVS is shown in Fig. 15. Note that, for the incompressible Navier–Stokes equations with the rigid wall assumption, the pressure is determined to be apart from an arbitrary constant. The Neumann (or natural) boundary condition for the SEM implies that the outlet pressure is zero.

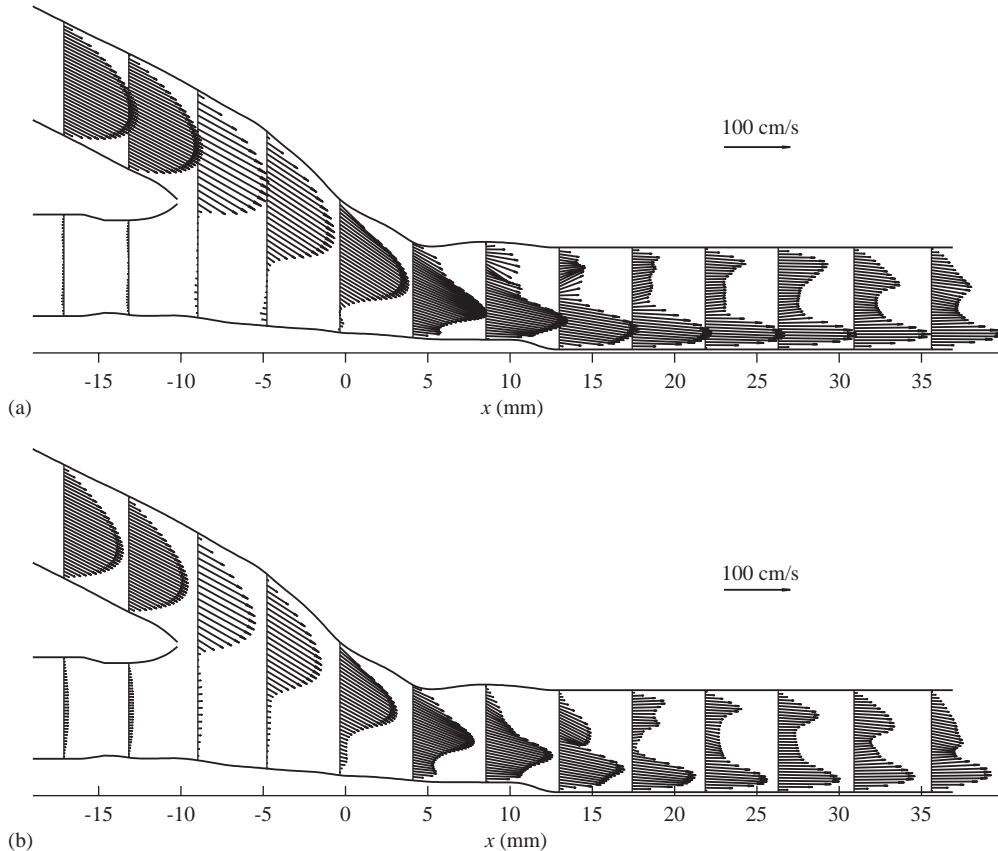


Fig. 7. Velocity vectors in the mid-plane during (a) maximum flow rate and (b) minimum flow rate.

5. Discussion

This paper presents *in vivo* VWV data and computational fluid dynamics simulations for unsteady flow in an AV graft. This work is a continuation of an ongoing study to elucidate the flow conditions that lead to the tissue vibration reported by [Fillinger et al. \(1990\)](#) and our group ([Loth et al., 2003](#)), with the ultimate goal of understanding the role of hemodynamics in AV graft failure. Our previous simulations ([Loth et al., 2003](#); [Lee et al., 2002b](#)), which were under steady flow conditions and based on an idealized symmetric model of the venous anastomosis, indicated that turbulence may play a role in the generation of VWV. In order to correlate the VWV with the hemodynamics, the present simulations were based on the graft *in vivo* geometry and pulsatile flow waveform on which VWV measurements were obtained. While velocity and pressure fluctuations are clearly present in the numerical simulations, their magnitude and frequency do not correlate well with the *in vivo* VWV measurements. In this section, potential reasons for this discrepancy are discussed.

The time traces and frequency spectra of the measured VWV ([Figs. 4 and 5](#)) clearly indicate significant wall motion in the range of 100–200 Hz and increasing magnitude moving downstream of the venous anastomosis ([Fig. 6](#)) in a manner consistent with the development of transitional flow vortices, as previously reported by [Loth et al. \(2003\)](#). The vein-wall displacement obtained by integration of the VWV traces ([Fig. 4](#)) is shown in [Fig. 16](#). The high-frequency component of the displacement, shown in [Fig. 16\(b\)](#), was obtained by applying a 40 Hz high-pass filter. The low-frequency displacement at locations $-10, 0, +10$ mm is approximately $\pm 50 \mu\text{m}$ and clearly follows the cardiac cycle with increasing magnitude further downstream. The high-frequency displacement ranges from approximately $\pm 5 \mu\text{m}$ at -10 mm to $\pm 15 \mu\text{m}$ at $+10$ mm. We note that [Loth et al. \(2003\)](#) reported similar displacements in the low-frequency range, but found significantly smaller ($< 1 \mu\text{m}$) displacement in high-frequency range (40–800 Hz) on a porcine animal model.

The CFD simulation was based on the pulsatile waveform of [Fig. 3](#). The computed flow field was determined to be laminar. The velocity and pressure time traces ([Figs. 10 and 12](#)) were completely repeatable from cycle to cycle during

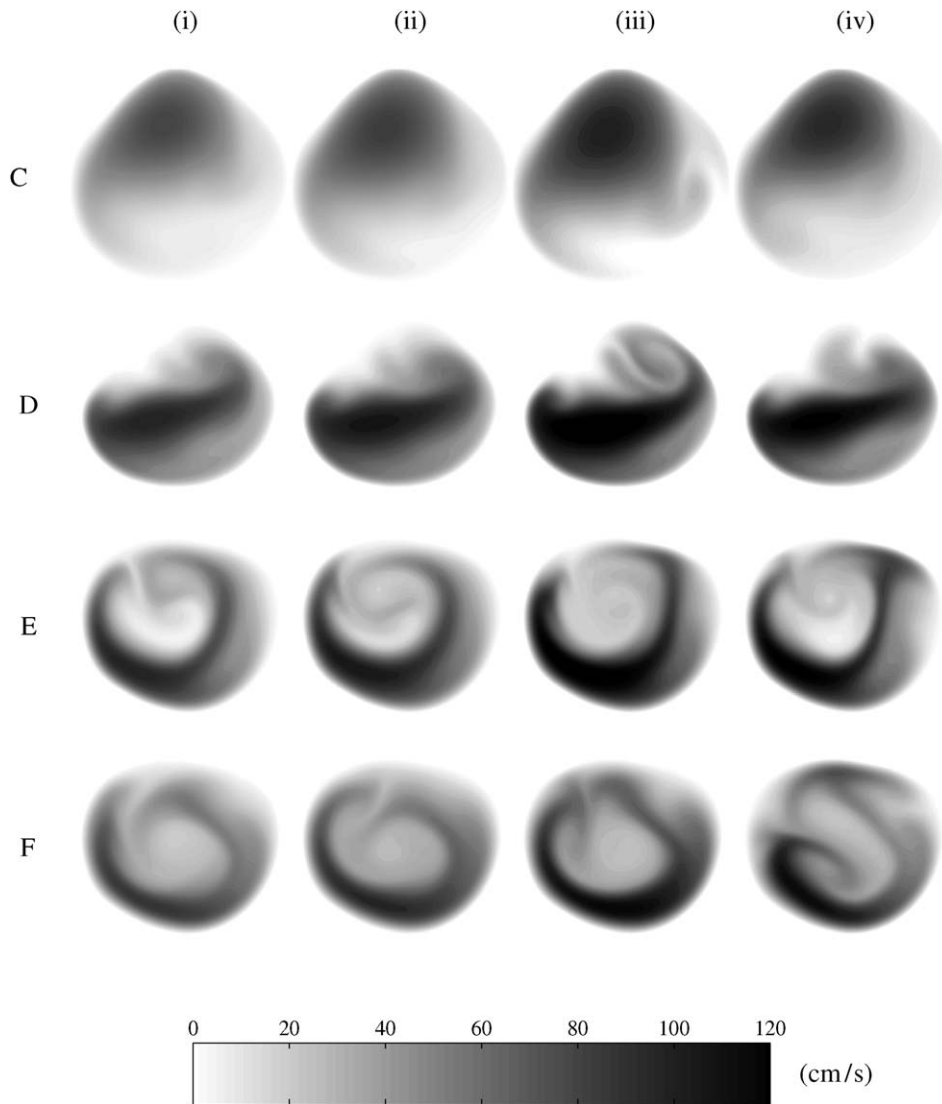


Fig. 8. The axial velocity magnitude at various locations (C–F in Fig. 1) and at various flow phases: (i) minimum flow rate; (ii) mid-acceleration; (iii) maximum flow rate; (iv) mid-deceleration (see Fig. 3).

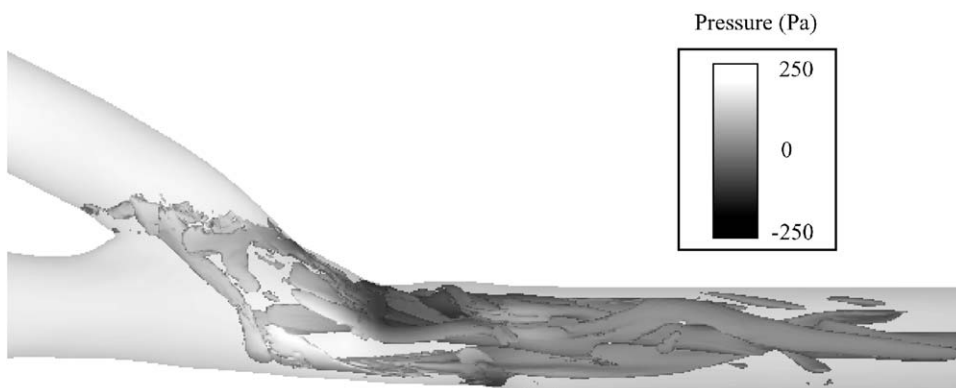


Fig. 9. Coherent structures represented at peak systole by using the λ_2 criterion (Jeong and Hussain, 1995).

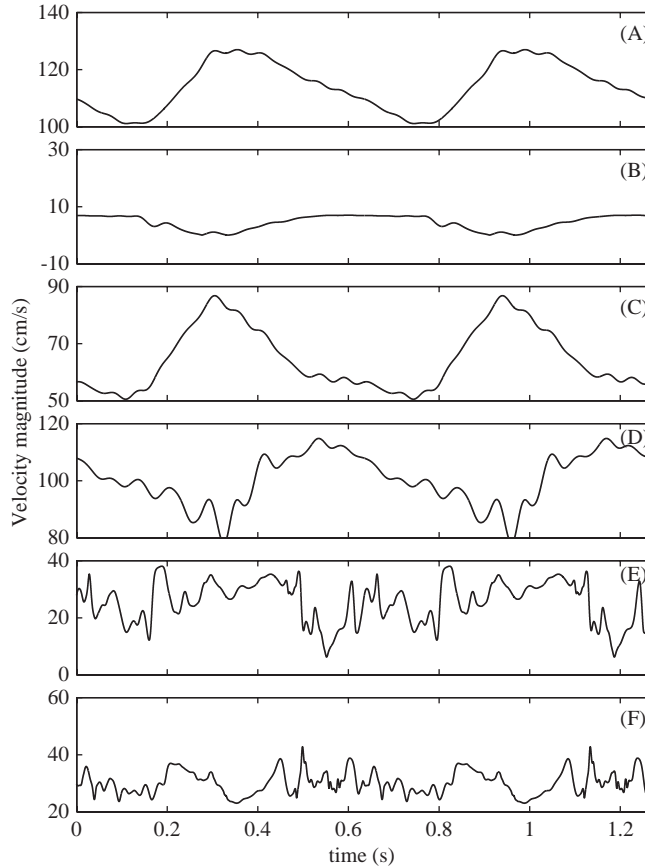


Fig. 10. Time traces of velocity magnitude at six streamwise locations (A–F in Fig. 1) for two cardiac cycles. Note the repeatability of the velocity traces between cycles even at positions E and F.

the six cycles of simulation time, indicating a lack of the irregularity that is characteristic of turbulence. Moreover, the coherent structures of Fig. 9 show no signs of transverse (or hairpin) vortices that are often associated with transitional flow [see Loth et al. (2003)]. Nonetheless, the velocity and pressure fluctuations of Figs. 10 and 12 do indicate an increase in high-frequency content that could possibly be identified with a transfer of energy to small scales. While these fluctuations are significant, their magnitude at frequencies above 30 Hz is rather small, in marked contrast to the VWV power spectrum at +10 mm (Fig. 5). The lack of high-frequency fluctuations observed in the CFD has been confirmed in steady-flow experiments using LDA on the same geometry at $Re = 1200$. Thus, we are confident that, under the modeled conditions, this flow does not transition to a turbulent state. We note that these results are consistent with Loth et al. (2003), who report transition at a graft Reynolds number of $Re_{\text{Graft}} = 1820$ ($Re_{\text{DVS}} = 2912$) and no transition at $Re_{\text{Graft}} = 1160$ ($Re_{\text{DVS}} = 1696$) for an idealized geometry under steady inlet conditions. While the present case is a more complex geometry and under pulsatile conditions, the behavior at the Reynolds number considered (maximum $Re_{\text{Graft}} \sim 1200 \sim \text{maximum } Re_{\text{DVS}}$) appears close to that of the laminar case reported by Loth et al. (2003). Note that the grid density employed in the present simulations was essentially the same as that used in our previous study in an idealized AV graft model (Loth et al., 2003). Thus, we are confident that the grid employed in this pulsatile study was sufficiently resolved to capture small-scale structures that would be present.

The discrepancies between the computed fluctuations and the measured in vivo VWV are striking, although we acknowledge that the geometric variation related to uncertainties in the casting technique presents a possible difference in conditions between the CFD model and the in vivo LDV measurements. The former (Figs. 11 and 13) indicates an absence of strong fluctuations at > 100 Hz, while the latter (Fig. 5) clearly indicates a spectral peak at ~ 200 Hz. While the reason for the discrepancies is unknown at present, three potential causes are described. First, the differences may be

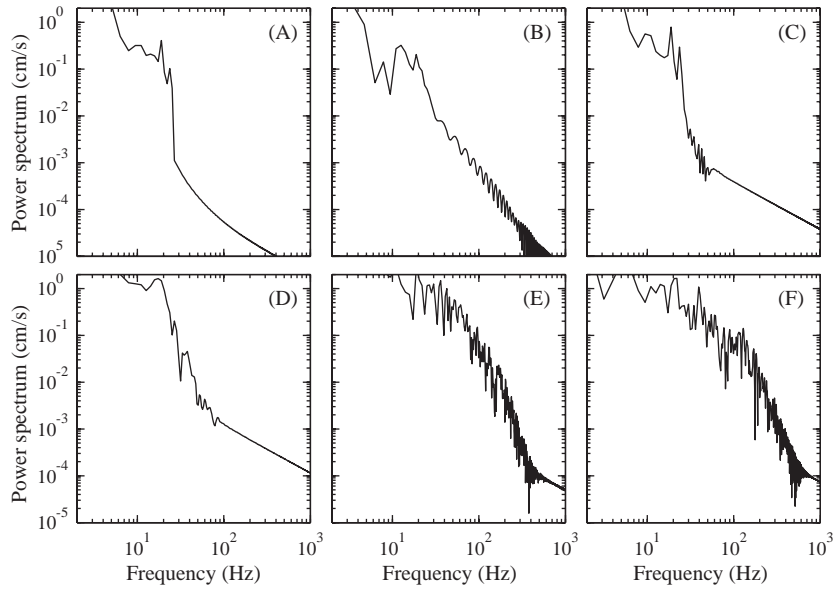


Fig. 11. Frequency spectra of velocity magnitude corresponding to the time traces in Fig. 10.

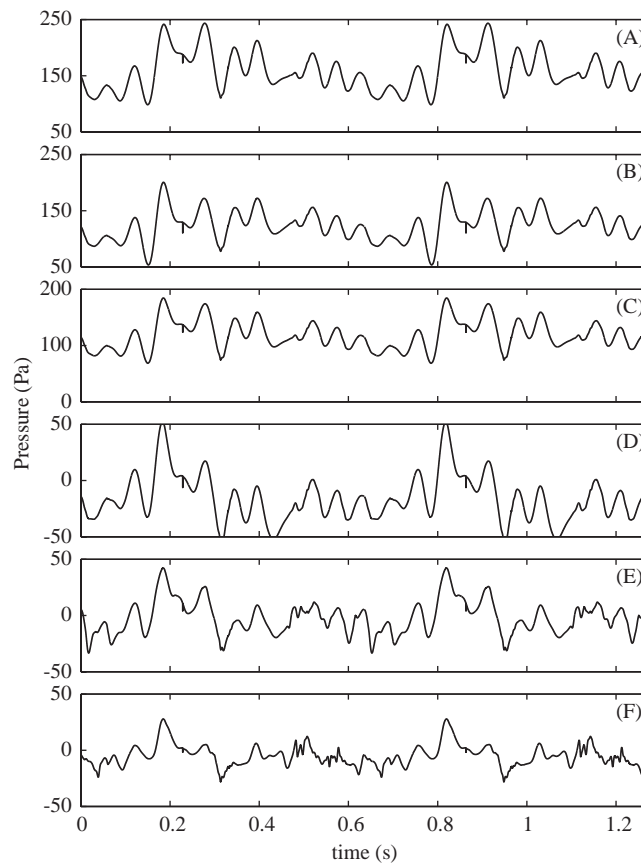


Fig. 12. Time trace of pressure at six streamwise locations (A–F in Fig. 1) for two cardiac cycles. Note the repeatability of the pressure traces between cycles even at positions E and F.

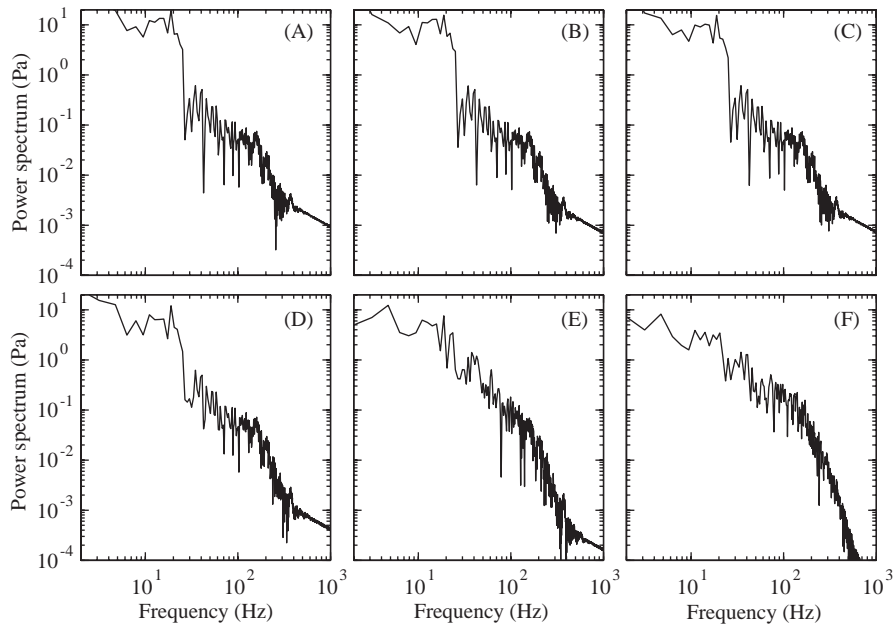


Fig. 13. Frequency spectra of pressure corresponding to the time traces in Fig. 12.

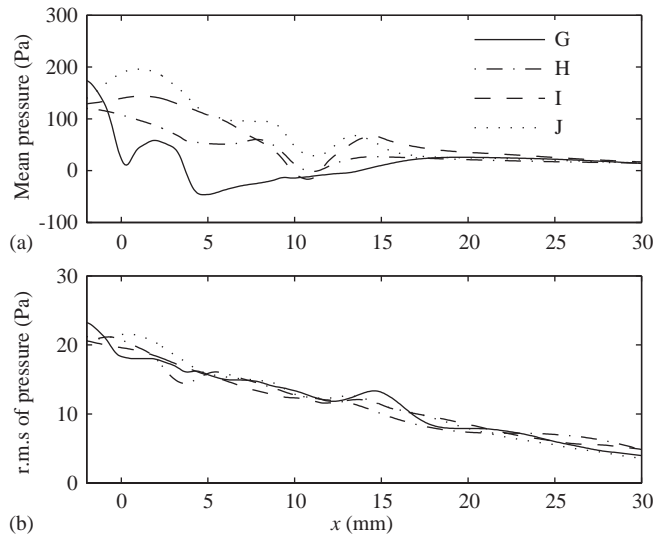


Fig. 14. Axial distribution of (a) time averaged and (b) r.m.s. of pressure at four circumferential locations (G–J in Fig. 1).

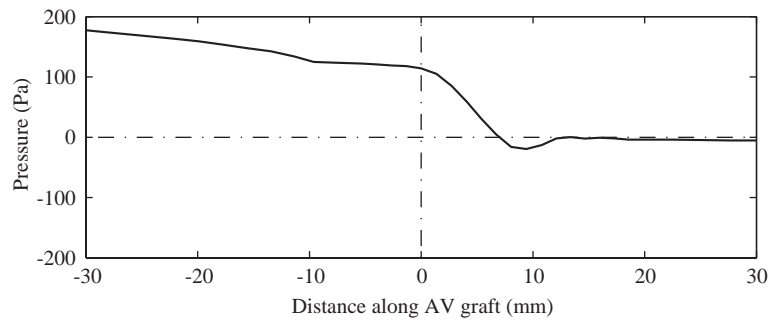


Fig. 15. Pressure distribution of time averaged at center locations of cross sections in streamwise direction from graft to PVS.

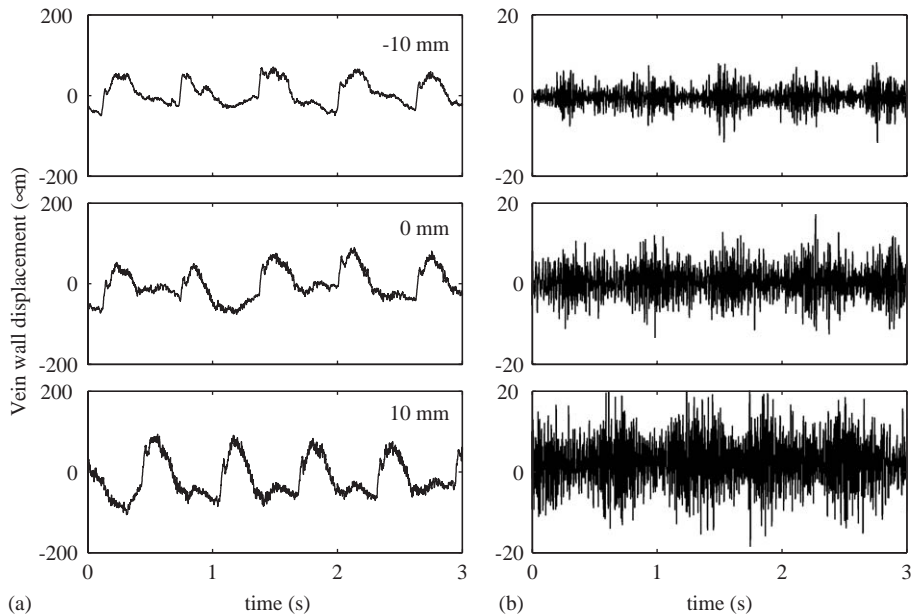


Fig. 16. Time trace of vein-wall displacement by integration of VWV velocity in vivo after graft construction: (a) nonfiltered; (b) band-pass filtered >40 Hz.

due to the quiescent inflow condition used in the present computations. A more realistic inflow condition might alter the velocity fluctuations significantly. However, a preliminary CFD study, in which the flow in the arterial anastomosis (AA) was simulated and then fed into the PTFE graft, indicated that turbulence generated in the AA is not sustained through the 20 cm PTFE graft segment at $Re_{\text{Graft}} = 1200$. In addition, the phase-averaged flow loses the detail of the individual flow waveform in each cycle, as shown in Fig. 3. This detailed temporal variation of a real flow waveform might affect the generation of turbulence. Moreover, the AV graft loop has a U-bend shape, as shown Fig. 1. Thus, the inflow would have a velocity profile skewed outward (Dean flow) rather than an axisymmetric profile of Womersley flow. However, a preliminary simulation of steady flow showed no differences in velocity fluctuations between a skewed outward inlet velocity and one that was parabolic.

Second, the present simulations were conducted assuming AV graft has rigid walls. Admittedly, fluid–structure interaction (FSI) would play an important role in the response of VWV. Simulations considering compliant wall motion have been reported over the past decade. However, most of these computations remained in the laminar flow regime (Dumont et al., 2004; Migliavacca et al., 2002; Tang et al., 2003) or simple geometry such as planar channel flow (Endo and Himeno, 2002; Xu et al., 2003; Yeo et al., 2001). FSI analysis of blood and vein wall motion is complex because of the transitional nature of the flow, complex geometry, pulsatile flow conditions, and viscoelastic properties of vessel walls. Hansen et al. (1987) suggested that the only wall vibration of the order of the viscous sublayer thickness could affect the turbulent flow and hypothesized that turbulent pressure fluctuations computed on a rigid wall may be applied as the exciting forces in structural vibration analysis. In addition, Xu et al. (2003) demonstrated by direct numerical simulation over compliant surface that a compliant surface has little effect on the turbulent skin friction and on the near-wall turbulent coherent structures. Many experimental and numerical works even reported that transition to turbulence could be delayed through the use of properly designed compliant wall (Davies and Carpenter, 1997; Carpenter et al., 2000). Thus, this simulation based on the rigid-wall assumption might seem to be reasonable and would have potential for providing significant information about turbulence-induced VWV because the PTFE and vein are less compliant than arteries under these pressure conditions (Brossollet, 1992). However, the effect on flow stability as a result of compliance under AV graft flow conditions is not well known. In addition, the rigid-wall assumption does not capture any dynamic FSI that may occur, including flow-induced instabilities of the vessel wall (Grotberg and Jensen, 2004).

Third, the flow split between the graft and the DVS may have an important effect on flow fluctuations. In the present case, the flow in the DVS was small ($<5\%$ of graft). Recent preliminary computations, however, have indicated that the stability of the PVS flow can be sensitive to the flow split between the PVS and DVS. It is also possible that the

disturbances downstream of the toe could propagate upstream via the wall and/or fluid to create some VWV in the DVS as observed in vivo. Since our CFD model assumes rigid walls, we are unable to observe this effect.

Secondary flow can also influence the onset of turbulence. While our calculations show no sign of transition, secondary flow is clearly evidenced by the coherent structures in Fig. 9. In the present computations, the axial flow profiles became “M” shaped one diameter after entering the PVS side of the vein. These profiles were significantly skewed toward the floor of the anastomosis, as shown in Fig. 7. This result is similar to that reported previously for flow in a graft geometry (Shu and Hwang, 1991; Ethier et al., 2000), but it contrasts with that reported by Loth et al. (2003) and Arslan (1999). These differences reflect the importance of geometry on the fluid dynamics and emphasize the fact that caution must be exercised when extrapolating results from one graft geometry to another.

The distribution of pressure is also of interest in AV grafts, because the pressure drop along the graft can be significant (Tricht et al., 2004). The pressure varies significantly in the circumferential direction for as much as two diameters downstream of the toe (see Fig. 14). The average axial pressure shows a decrease of almost 200 Pa (~ 1.5 mmHg) within a distance of 30 mm in the graft and PVS. This indicates the significant shear stresses within the graft under these flow conditions. Better understanding of why the vein wall vibrates may lead to design changes in the graft construction that could improve the longevity of these vascular constructs and thus reduce AV graft failure rate.

6. Conclusion

The present work presents a CFD study for a subject-specific AV-graft geometry using a realistic pulsatile flow waveform in order to elucidate the fluid dynamics responsible for VWV. While the CFD results show some fluctuations in velocity and pressure, these are not in the frequency range of the measured in vivo VWV. Several possible reasons for this discrepancy are identified, including inlet flow conditions, rigid wall assumption, and effect of flow split. Further research studies need to be conducted to determine the relative importance of each possible cause.

Acknowledgments

We thank Wojciech Kalata and David S. Smith for their help on the image processing, Seung E. Lee for his previous work on the meshing algorithm, Henry Tufo for assistance with the simulations, and Jim Vosicky for his help on the animal study. This work was supported by the Whitaker Foundation (RG-01-0198); National Institutes of Health, RO1 Research Project Grant (2RO1HL55296-04A2); R21 Research Project Grant (1R21EB002511-01); the Mathematical, Information, and Computational Sciences Division subprogram of the Office of Advanced Scientific Computing Research, Office of Science, US Department of Energy, under Contract W-31-109-Eng-38; and NSF Pittsburgh Supercomputing Center. This work was also supported in part by W.L. Gore & Associates.

References

- Arslan, N., 1999. Experimental characterization of transitional unsteady flow inside a graft-to-vein junction. Ph.D. Thesis. Department of Mechanical and Industrial Engineering, University of Illinois at Chicago, Chicago, USA.
- Boughner, D.R., Roach, M.R., 1971. Effect of low frequency vibration on the arterial wall. *Circulation Research* 29, 136–144.
- Brossollet, L.J., 1992. Effects of cryopreservation on the biaxial mechanical properties of canine saphenous veins. Ph.D. Thesis. Department of Mechanical Engineering, Georgia Institute of Technology, Atlanta, USA.
- Carpenter, P.W., Davies, C., Lucey, A.D., 2000. Hydrodynamics and compliant walls: Does the dolphin have a secret? *Current Science* 79, 758–765.
- Davies, C., Carpenter, P.W., 1997. Numerical simulations of the evolution of Tollmien–Schlichting waves over finite compliant panels. *Journal of Fluid Mechanics* 335, 361–392.
- Dumont, K., Stijnen, J.M., Vierendeels, J., van de Vosse, F.N., Verdonck, P.R., 2004. Validation of a fluid-structure interaction model of a heart valve using the dynamic mesh method in fluent. *Computational Methods in Biomechanics and Biomedical Engineering* 7, 139–146.
- Endo, T., Himeno, R., 2002. Direct numerical simulation of turbulent flow over a compliant surface. *Journal of Turbulence* 3, 1–10.
- Ene-Iordache, B., Mosconi, L., Remuzzi, G., Remuzzi, A., 2001. Computational fluid dynamics of a vascular access case for hemodialysis. *ASME Journal of Biomechanical Engineering* 123, 284–292.
- Ethier, C.R., Prakash, S., Steinman, D.A., Leask, R.L., Couch, G.G., Ojha, M., 2000. Steady flow separation patterns in a 45 degree junction. *Journal of Fluid Mechanics* 411, 1–38.

- Evangelinos, C., Karniadakis, G.E., 1999. Dynamics and flow structures in the turbulent wake of rigid and flexible cylinders subject to vortex-induced vibrations. *Journal of Fluid Mechanics* 400, 91–124.
- Fillinger, M.F., Reinitz, E.R., Schwartz, R.A., Resetarits, D.E., Paskanik, A.M., Brunch, D., Bredenberg, C.E., 1990. Graft geometry and venous intimal-medial hyperplasia in arteriovenous loop grafts. *Journal of Vascular Surgery* 11, 556–566.
- Fischer, P.F., 1997. An overlapping Schwarz method for spectral element solution of the incompressible Navier–Stokes equations. *Journal of Computational Physics* 133, 84–101.
- Fischer, P.F., Kruse, G.W., Loth, F., 2002. Spectral element methods for transitional flows in complex geometries. *ASME Journal of Scientific Computing* 17, 81–98.
- Foreman, J.E., Hutchison, K.J., 1970. Arterial wall vibration distal to stenoses in isolated arteries of dog and man. *Circulation Research* 26, 583–590.
- Grotberg, J.B., Jensen, O.E., 2004. Biofluid mechanics in flexible tubes. *Annual Review of Fluid Mechanics* 36, 121–147.
- Guilmineau, E., Queutey, P., 2000. A numerical simulation of the response of a vortex excited cylinder. In: Ziada, S., Staubli, T. (Eds.), *Proceedings of the Seventh International Conference on Flow Induced Vibration*. Balkema, Rotterdam, Netherlands, pp. 257–264.
- Hansen, R.J., Handler, R.A., Leighton, R.I., Orszag, S.A., 1987. Prediction of turbulence-induced forces on structures from full numerical solutions of the Navier–Stokes equations. *Journal of Fluids and Structures* 1, 431–443.
- Jeong, J., Hussain, F., 1995. On the identification of a vortex. *Journal of Fluid Mechanics* 285, 69–94.
- Kanterman, R.Y., Vesely, T.M., Pilgram, T.K., Guy, B.W., Windus, D.W., Picus, D., 1995. Dialysis access grafts: anatomic location of venous stenosis and results of angioplasty. *Radiology* 195, 135–139.
- Lee, S.E., 2002. Solution method for transitional flow in a vascular bifurcation based on in vivo medical images. M.S. Thesis. Department of Mechanical and Industrial Engineering, University of Illinois at Chicago, Chicago, USA.
- Lee, S. E., Piersol, N., Loth, F., Fischer, P. F., Leaf, G., Smith, B., Yedavalli, R., Yardimci, A., Alperin, N., Schwartz, L., 2000. Automated mesh generation of an arterial bifurcation based upon in vivo MR images. *Digest of Papers of the 2000 World Congress on Medical Physics and Bioengineering, MO-G326*, Chicago, USA.
- Lee, S.E., Loth, F., Fischer, P.F., 2002a. Unstructured hexahedral mesh based on conduction temperature distribution. *Proceedings CD of the Fourth World Congress of Biomechanics, Calgary, Canada*.
- Lee, S.-W., Loth, F., Royston, T.J., Fischer, P.F., Shaalan, W.E., Bassiouny, H.S., 2002b. Turbulence induced vein-wall vibration may play a role in arteriovenous dialysis graft failure. *Proceedings CD of the Fourth World Congress of Biomechanics, Calgary, Canada*.
- Loth, F., Fischer, P.F., Arslan, N., Bertram, C.D., Lee, S.E., Royston, T.J., Shaalan, W.E., Bassiouny, H.S., 2003. Transitional flow at the venous anastomosis of an arteriovenous graft: potential activation of the ERK1/2 mechanotransduction pathway. *Journal of Biomechanical Engineering* 125, 49–61.
- Maday, Y., Patera, A.T., 1989. Spectral element methods for the Navier–Stokes equations. In: Noor, A.K., Oden, J.T. (Eds.), *State-of-the-Art Surveys in Computational Mechanics*. ASME, New York, pp. 71–143.
- Maday, Y., Patera, A.T., Rønquist, E.M., 1990. An operator-integration-factor splitting method for time-dependant problems: application to incompressible fluid flow. *Journal of Scientific Computing* 5, 263–292.
- Mallinger, F., Drikakis, D., 2002. Laminar-to-turbulent transition in pulsatile flow through a stenosis. *Biorheology* 39, 437–441.
- Migliavacca, F., Pennati, G., Di Martino, E., Dubini, G., Pietrabissa, R., 2002. Pressure drops in a distensible model of end-to-side anastomosis in systemic-to-pulmonary shunts. *Computational Methods in Biomechanics and Biomedical Engineering* 5, 243–248.
- Mittal, S.P., Simmons, S.P., Najjar, F., 2003. Numerical study of pulsatile flow in a constricted channel. *Journal of Fluid Mechanics* 485, 337–378.
- Ojha, M., Langille, B.L., 1993. Evidence that turbulence is not the cause of poststenotic dilatation in rabbit carotid arteries. *Arteriosclerosis and Thrombosis* 13, 977–984.
- Roach, M.R., 1963. An experimental study of the production and time course of poststenotic dilatation in the femoral and carotid arteries of adult dogs. *Circulation Research* 13, 537–551.
- Shiels, D., Leonard, A., Roshko, A., 2001. Flow induced vibration of a circular cylinder at limiting structural parameters. *Journal of Fluids and Structures* 15, 3–21.
- Shu, M.C.S., Hwang, N.H.C., 1988. Flow phenomena in compliant and noncompliant arteriovenous graft. *Transactions American Society for Artificial Internal Organs* 34, 519–523.
- Shu, M.C.S., Hwang, N.H.C., 1991. Haemodynamics of angioaccess venous anastomoses. *Journal of Biomedical Engineering* 13, 103–112.
- Shu, M.C.S., Noon, G.P., Hwang, N.H.C., 1987. Flow profiles and wall shear stress distribution at a hemodialysis venous anastomosis: preliminary study. *Biorheology* 24, 723–735.
- Sivanesan, S., How, T.V., Black, R.A., Bakran, A., 1999. Flow patterns in the radiocephalic arteriovenous fistula: an in vitro study. *Journal of Biomechanics* 32, 915–925.
- Tang, D., Yang, C., Kobayashi, S., Zheng, J., Vito, R.P., 2003. Effect of stenosis asymmetry on blood flow and artery compression: a three-dimensional fluid-structure interaction model. *Annals of Biomedical Engineering* 31, 1182–1193.
- Tricht, I.V., Wachter, D.D., Tordoir, J., Verdonck, P., 2004. Hemodynamics in a compliant hydraulic in vitro model of straight versus tapered PTFE arteriovenous graft. *Journal of Surgical Research* 116, 297–304.
- Womersley, J.R., 1957. An elastic tube theory of pulse transmission and oscillatory flow in mammalian arteries. Technical Report WADC-TR-56-614, Wright Air Development Center, Dayton, USA.

- Xu, S., Rempfer, D., Lumley, J., 2003. Turbulence over a compliant surface: numerical simulation and analysis. *Journal of Fluids Mechanics* 478, 11–34.
- Yedavalli, R.V., Loth, F., Yardimci, A., Pritchard, W.F., Oshinski, J.N., Sadler, L., Charbel, F., Alperin, N., 2001. Construction of a physical model of the human carotid artery based upon in vivo magnetic resonance images. *Journal of Biomechanical Engineering* 123, 372–376.
- Yeo, K.S., Zhao, H.Z., Khoo, B.C., 2001. Turbulent boundary layer over a compliant surface: absolute and convective instabilities. *Journal of Fluid Mechanics* 449, 141–168.